Bayesian inference for generalized extreme value distribution with Gaussian copula dependence

Bo Ning

Department of Statistics, North Carolina State University
and
Peter Bloomfield
Department of Statistics, North Carolina State University

March 6, 2017

Abstract

Dependent generalized extreme value (dGEV) models have attracted much attention due to the dependency structure that often appears in real datasets. To construct a dGEV model, a natural approach is to assume that some parameters in the model are time-varying. A previous study has shown that a dependent Gumbel process can be naturally incorporated into a GEV model. The model is a nonlinear state space model with a hidden state that follows a Markov process, with its innovation following a Gumbel distribution. Inference may be made for the model using Bayesian methods, sampling the hidden process from a mixture normal distribution, used to approximate the Gumbel distribution. Thus the response follows an approximate GEV model. We propose a new model in which each marginal distribution is an exact GEV distribution. We use a variable transformation to combine the marginal CDF of a Gumbel distribution with the standard normal copula. Then our model is a nonlinear state space model in which the hidden state equation is Gaussian. We analyze this model using Bayesian methods, and sample the elements of the state vector using particle Gibbs with ancestor sampling (PGAS). The PGAS algorithm turns out to be very efficient in solving nonlinear state space models. We also show our model is flexible enough to incorporate seasonality.

Keywords: Generalized extreme value; nonlinear state space model; particle Gibbs sampler; time series analysis.

1   Introduction

Generalized extremely value models have been used extensively to estimate and predict extreme events in many applications, for instance in the environment, engineering, economics and finance.

The theoretical properties of this model have been studied in the literature (Pickands, 1975; Castillo et al., 2004). Both frequentist and Bayesian approaches have been developed to estimate those models (Coles, 2001; Coles and Powell, 1996). Recently, dependent GEV models (for short, dGEV models) have attracted much attention. Those models are useful in applications when extreme events are time-correlated. For example, higher temperature in one day may be followed by a higher temperature in another day.

A GEV distribution is shown as follows:

$$P(Y \leq y) = F(y) = \exp\left\{-\left(1 + \xi\frac{y - \mu}{\psi}\right)_+^{-\frac{1}{\xi}}\right\}, \tag{1.1}$$

where μ, ψ and ξ are the location, scale and shape parameters respectively. To extend the GEV model to a dGEV model, it is common to introduce dependence for some of its parameters. Previous studies have focused on letting μ follow an AR(1) process with other parameters time invariant (Huerta and Sansó, 2007); and letting μ, ψ and ξ be time-dependent and follow ARMA-type process (Wei and Huerta, 2016). However, since we consider the dependency of extreme events, a more general way to introduce the time-dependent structure is to insert a copula; this idea is originally proposed by Nakajima et al. (2011, 2015). To be explicit, their model is constructed as follows.

If we define

$$\alpha_t \equiv \log\left\{\left(1 + \xi\frac{Y_t - \mu}{\psi}\right)_+^{\frac{1}{\xi}}\right\}, \tag{1.2}$$

then α_t follows the Gumbel distribution. Solving (1.2) for Y_t, we find the following expression,

$$Y_t = \mu + \psi\frac{\exp(\xi\alpha_t) - 1}{\xi}, \tag{1.3}$$

and if α_t is a hidden AR(1) process,

$$\alpha_{t+1} = \phi\alpha_t + \eta_t, \quad \eta_t \sim \text{Gumbel}, \tag{1.4}$$

then the model becomes a nonlinear non-Gaussian state space model. To estimate the parameters in the model, they first show that the model can be approximated by a linear Gaussian state space model, by finding a linear approximation for nonlinear observation equations and using

mixed normal distributions to approximate the Gumbel errors in the state equation. However, from (1.4) the marginal distribution of α_t does not follow a Gumbel distribution, because the sum of two Gumbel-distributed random variables in general does not follow a Gumbel distribution. We propose a method to allow α_t to follow exactly the Gumbel distribution. The model has Gumbel marginal distributions linked together with a Gaussian copula with AR(1) dependence. By this construction, the marginal distribution of α_t is exactly from a Gumbel distribution. The details are shown in Section 2.

Because the number of variables in the dGEV model is large, we use Bayesian analysis to sample draws from the joint distributions. Markov chain Monte Carlo (MCMC) allows us to sample from the conditional distribution for each individual parameter, and thus we only need to take care of the conditional distribution of each parameter at one time instead of the joint distribution for all parameters. A drawback of using the MCMC algorithm is that the mixing can be slow due to the high dimensional state vector in the model. As a result, many iterations are needed and methods to reduce the correlation between chains such as marginalization, permutation and trimming (Dyk and Park, 2008; Liu et al., 1994; Liu, 1994) must be considered.

In Bayesian analysis, a common technique is to use Kalman filtering and backward smoothing (KFBS) (West and Harrison, 1997) for sampling draws from linear Gaussian state space models. For nonlinear non-Gaussian state space models, the KFBS cannot applied directly. One way of sampling those model is to find a linear approximation for the nonlinear equations (Shephard and Pitt, 1997); common techniques include using a first-order Taylor series expansion based on the observation equations, or a second-order Taylor expansion based on the log-likelihood functions, and finding a mixed normal approximation for the non-Gaussian errors. The sampling approach is to apply KFBS algorithm on the approximated linear Gaussian state space model, and using Metropolis-Hastings (M-H) to accept or reject the draws. However, When the model is highly nonlinear and non-Gaussian these approximation techniques may perform very poorly; as a result, the M-H step will reject most of the draws, thus increasing the computation time and reducing the mixing rate of the chain. There are many extensions for the KFBS for adapting to a nonlinear state space model including extended Kalman filter, robust extended Kalman filter (Einicke and White, 1999) and using mixed normal densities to approximate nonGaussian densities (Niemi and West, 2010).

An alternative way to make inferences in a nonlinear state space model is by using sequential Monte Carlo (SMC). This approach is as follows: it first generates particles from a chosen proposal density; and then calculate the weights between the proposal density and the true density. The generated particles and their weights give a discrete distribution approximation to the true density. However, one issue with this method is the degeneration of the weights, thus a resampling step is needed when calculating the weights. This method is also known as importance sampling. Recently, much effort has been put into incorporating SMC within MCMC; some of the methods include particle Metropolis-Hastings and the particle Gibbs sampler (Andrieu et al., 2010). To use MCMC approach is more convenient when dealing with a model with many variables. The particle Gibbs sampler is the method we shall use in this paper; this method uses collapsed Gibbs sample (Liu, 1994), which allows the joint distribution to be invariant in MCMC sampling. The essential idea is to combine a conditional SMC (cSMC) (Liu, 2001) with the Gibbs sampler. The cSMC method needs to keep a path known as ancestor lineage to survive in each resampling step. However, this algorithm has two weaknesses: poor mixing rate and particle degeneration (Doucet and Johansen, 2011; Chopin and Singh, 2015). An extension to address these weaknesses is to do backward smoothing, which known as forward sampling and backward smoothing (FFBS) (Whiteley, 2010; Lindsten and Schön, 2013; Kantas et al., 2015). A drawback for the FFBS algorithm is that adding the backward step increases the computation time. A more recent method which is known as Particle Gibbs with ancestor sampling (PGAS) (Lindsten et al., 2014) is proposed to address the computation issues of FFBS. The PGAS approach is as follows: for each forward sampling step, instead of fixing the ancestor lineage, the algorithm resamples the ancestor lineage. In this case, some particles with small weights in the ancestor lineage will drop out.

In the rest of the paper, we will introduce our novel dGEV model, which incorporates the dependence between extreme events through a dependent Gumbel distribution; the dependent Gumbel distribution is constructed with a normal copula, and in the final model the observed variable is sampled from an exact GEV distribution. Our model can be expressed as a nonlinear Gaussian state space model; we use PGAS to sample the hidden process in the nonlinear state space model. We also show that our model may be extended to incorporate seasonal components, which are needed for some datasets; we name the result a seasonal dGEV model.

In the simulation study, we show our estimated posterior medians for parameters are close to the true values, and the true values are contained in the 95% credible intervals. Because the latent variables marginally follow a standard normal distribution, we could use standard normal distribution tails to characterize the extremeness of the values.

We fit the model to two real datasets: one is an annual maximum water flow dataset and the other is a weekly minimum return for the S&P 500 index.

The remaining sections are arranged as follows: Section 2 introduces our dGEV model; Section 3 describes a Bayesian computation steps; Section 4 adds seasonality on the dGEV model; Section 5 illustrates the dGEV and seasonal dGEV models using simulated data; Section 6 conducts a real data study for a water flow dataset and a financial dataset; Section 7 concludes.

2   The dGEV model.

Our dGEV model is constructed as follows: suppose that β_t follows the standard normal distribution, so that $\Phi(\beta_t)$ follows the uniform $(0,1)$ distribution. Let $G(\alpha)$ be the CDF of the Gumbel distribution: $G(\alpha) = \exp(-\exp(-\alpha))$. If

$$\alpha_t = G^{-1}(\Phi(\beta_t)) = -\log(-\log(\beta_t)),$$

then α_t follows the Gumbel distribution.

Now suppose that β_t follows an AR(1) process:

$$\beta_{t+1} = \phi\beta_t + \eta_t, \quad \text{where } \eta_t \sim N(0, 1-\phi^2) \tag{2.1}$$

for $t = 1, \ldots, T-1$ and $\beta_1 \sim N(0,1)$, and let

$$
\begin{aligned}
Y_t &= \mu + \psi\frac{\exp(\xi\alpha_t) - 1}{\xi} + \epsilon_t \\
&= \mu + \psi\frac{(-\log(\Phi(\beta_t)))^{-\xi} - 1}{\xi} + \epsilon_t, \quad \epsilon_t \sim N(0, \sigma^2)
\end{aligned}
\tag{2.2}
$$

where $t = 1, \ldots, T$ and $\beta_1 \sim N(0,1)$. The normal error ϵ_t in the observation equation is a added term that makes the model have a nonlinear state space presentation; the error should be have a

small variance to make it negligible.

The parameters in our model are μ, ψ, ξ, θ, σ^2 and the latent variables $\beta_{1:T}$. In Bayesian analysis, we adopt a similar priors for these parameters to those suggested by (Coles and Tawn, 1996; Chavez-Demoulin and Davison, 2012): $\mu \sim N(\nu_\mu, \sigma_\mu^2)$, $\psi \sim \mathrm{Gamma}(a_\psi, b_\psi)$, $\xi \sim N(\nu_\xi, \sigma_\xi^2)$. The prior for $\phi \sim U(-1, 1)$ to make sure the AR(1) process in (2.1) is stationary. Last, the prior for $\sigma^{-2} \sim \mathrm{InvGamma}(a, b)$, which we later abbreviate $\mathrm{IG}(a, b)$.

3   Posterior computation

In this section, we describe a MCMC algorithm for sampling draws of the parameters in the dGEV model. Because of the many parameters, a slow mixing rate will cause the chain converge very slowly. To ameliorate this problem, we consider using trimming and blocking techniques; Dyk and Park (2008) have justified those techniques as useful.

In the following, to simplify the notation, let $\boldsymbol{\theta}$ to be any parameter(s) in the model and $-\boldsymbol{\theta}$ to be the parameters in the model except $\boldsymbol{\theta}$. The outline of the MCMC algorithm is designed as follows: we sample $\pi_{-\boldsymbol{\vartheta}}(\boldsymbol{\vartheta}|\boldsymbol{Y})$ from its posterior distribution by grouping μ, ψ, and ξ together and treating them as a block; and then sample $\pi_{-\sigma^2}(\sigma^2|\boldsymbol{Y})$, $\pi_{-\phi}(\phi|\boldsymbol{Y})$ from the conditional posterior distribution using Gibbs and Metropolis-Hastings algorithm; last, sample $\pi_{-\boldsymbol{\beta}}(\boldsymbol{\beta}|\boldsymbol{Y})$ using particle Gibbs with ancestor sampler (PGAS), which will be introduced later.

3.1   Sampling μ, ψ, ξ

It is suggested to group μ, ψ, ξ parameters together and sample from their joint distribution to reduce the correlation between MCMC chains (Nakajima et al., 2011). Then the joint conditional posterior distribution for $\boldsymbol{\vartheta}$ is

$$\pi_{-\boldsymbol{\vartheta}}(\boldsymbol{\vartheta}|\boldsymbol{Y}) = \prod_{t=1}^{T} \pi_{-\boldsymbol{\vartheta}}(\boldsymbol{\vartheta}|Y_t)\pi(\mu)\pi(\psi)\pi(\xi) \tag{3.1}$$

Although the priors for $\boldsymbol{\mu}$ and $\boldsymbol{\psi}$ is conjugate with their likelihoods, the prior for $\boldsymbol{\xi}$ does not. When we group them as a trivariate parameters, the joint likelihood is not conjugacy with the priors, thus we use Metropolis-Hastings algorithm and find a proposal density using the second-

order Taylor expansion of $\log \pi_{-\boldsymbol{\vartheta}}(\boldsymbol{\vartheta}|\boldsymbol{Y})$ as follows. Let $\boldsymbol{\vartheta}^* \sim \text{MVN}(\boldsymbol{\nu}^*, \boldsymbol{\Sigma}^*)$, where

$$
\begin{aligned}
\boldsymbol{\Sigma}^{*-1} &= -\frac{\partial^2 \log \pi_{-\boldsymbol{\vartheta}}(\boldsymbol{\vartheta}|\boldsymbol{Y})}{\partial \boldsymbol{\vartheta} \, \partial \boldsymbol{\vartheta}^T}\bigg|_{\boldsymbol{\vartheta}=\hat{\boldsymbol{\vartheta}}}, \\
\boldsymbol{\nu}^* &= \hat{\boldsymbol{\vartheta}} + \boldsymbol{\Sigma}^* \cdot \frac{\partial \log \pi_{-\boldsymbol{\vartheta}}(\boldsymbol{\vartheta}|\boldsymbol{Y})}{\partial \boldsymbol{\vartheta}}\bigg|_{\boldsymbol{\vartheta}=\hat{\boldsymbol{\vartheta}}},
\end{aligned}
$$

and $\hat{\boldsymbol{\vartheta}}$ is a value that maximizes the posterior of $\pi_{-\boldsymbol{\vartheta}}(\boldsymbol{\vartheta}|\boldsymbol{Y})$; this value can be calculated by using optim in R. After sampling a draw $\boldsymbol{\vartheta}^*$ from this proposal density, we use Metropolis-Hastings to accept or reject $\boldsymbol{\vartheta}^*$ with ratio

$$
\alpha(\boldsymbol{\vartheta}, \boldsymbol{\vartheta}^*) = \min\left\{1, \frac{\pi_{-\boldsymbol{\vartheta}}(\boldsymbol{\vartheta}^*|\boldsymbol{Y})f(\boldsymbol{\vartheta}|\boldsymbol{\nu}^*, \boldsymbol{\Sigma}^*)}{\pi_{-\boldsymbol{\vartheta}}(\boldsymbol{\vartheta}|\boldsymbol{Y})f(\boldsymbol{\vartheta}^*|\boldsymbol{\nu}^*, \boldsymbol{\Sigma}^*)}\right\}.
$$

3.2 Sampling σ^2

To sample σ^2, we choose a conjugate prior inverse gamma prior as follows,

$$
\sigma^2 \sim \text{IG}(a, b).
$$

Since ϵ_t should be small, we choose a to be large and b to be small so that the prior will have a smaller variance.

The posterior of σ^2 can be written as follows:

$$
\pi_{-\sigma^2}(\sigma^2|\boldsymbol{Y}) = \text{IG}\left(a + \frac{T}{2}, b + \frac{\sum_{t=1}^{T}\left(y_t - \mu - \frac{\psi}{\xi}(-\log(\Phi(\beta_t))^{-\xi} - 1)\right)^2}{2}\right). \tag{3.2}
$$

3.3 Sampling ϕ

The conditional posterior of ϕ can be expressed as follows:

$$
\pi_{-\phi}(\phi|\boldsymbol{Y}) = (2\pi)^{-T/2}(1 - \phi^2)^{-T/2} \cdot \exp\left\{-\frac{\sum_{t=2}^{T}(\beta_t - \phi\beta_{t-1})^2}{2(1 - \phi^2)}\right\} \cdot \pi(\phi) \tag{3.3}
$$

where $\pi(\phi)$ is the prior of ϕ. Because the posterior density is not a well known distribution, similar to dealing with parameter $\boldsymbol{\vartheta}$, we find a proposal density for $\pi_{-\phi}(\phi|\boldsymbol{Y})$ as $q_{-\phi}(\phi|\boldsymbol{Y}) \sim N(\nu_\phi, \sigma_\phi^2)$

with

$$
\begin{aligned}
\sigma_\phi^{-2} &= -\frac{\partial^2 \log \pi_{-\phi}(\phi|\boldsymbol{Y})}{\partial \phi^2}\Big|_{\phi=\hat{\phi}}, \\
\nu_\phi &= \hat{\phi} + \sigma_\phi^2 \cdot \frac{\partial \log \pi_{-\phi}(\phi|\boldsymbol{Y})}{\partial \phi}\Big|_{\phi=\hat{\phi}}.
\end{aligned}
$$

After we draw $\phi^* \sim q_{-\phi}(\phi|\boldsymbol{Y}) \sim N(\nu_\phi, \sigma_\phi^2)$, ϕ^* is accepted with probability

$$
\alpha(\phi, \phi^*) = \min\left\{1, \frac{\pi_{-\phi}(\phi^*|\boldsymbol{Y})q_{-\phi}(\phi|\boldsymbol{Y})}{\pi_{-\phi}(\phi|\boldsymbol{Y})q_{-\phi}(\phi^*|\boldsymbol{Y})}\right\}.
$$

3.4 Sampling $\beta_{1:T}$

The posterior distribution for $\pi_{-\boldsymbol{\beta}}(\boldsymbol{\beta}|\boldsymbol{Y})$ can be expressed as the following,

$$
\pi_{-\boldsymbol{\beta}}(\boldsymbol{\beta}|\boldsymbol{Y}) = \prod_{t=1}^{T} f(Y_t|\beta_t, \boldsymbol{\vartheta}, \sigma^2) \prod_{t=2}^{T} f(\beta_t|\beta_{t-1}, \phi)\pi(\beta_1),
$$

with

$$
\begin{aligned}
f(Y_t|\beta_t, \boldsymbol{\vartheta}, \sigma^2) &= \left(\frac{1}{2\pi\sigma^2}\right)^{-\frac{T}{2}} \exp\left\{-\frac{Y_t - \mu - \frac{\psi}{\xi}((-\log(\Phi(\beta_t)))^{-\xi} - 1)}{2\sigma^2}\right\}, \\
f(\beta_t|\beta_{t-1}, \phi) &= \left(\frac{1}{2\pi(1-\phi^2)}\right)^{-\frac{T-1}{2}} \exp\left\{-\frac{\sum_{t=2}^{T}(\beta_t - \phi\beta_{t-1})^2}{2(1-\phi^2)}\right\}, \\
\pi(\beta_1) &= -\frac{1}{\sqrt{2\pi}} \exp\left\{-\frac{\beta_1^2}{2}\right\}.
\end{aligned}
$$

Due to the highly nonlinear expression of the likelihood $f(Y_t|\beta_t, \boldsymbol{\vartheta}, \sigma^2)$, the Kalman filter and backward smoothing algorithm developed based on linear state space models cannot be applied directly. That is because the linear approximation using Taylor expansion has very poor performance. As a result, the acceptance probability is almost 0 for our model.

The particle Gibbs sampler proposed by Andrieu et al. (2010) provides an alternative to sampling the nonlinear state space model. It is based on the conditional sequential Monte Carlo (cSMC) (Liu, 2001) algorithm which is similar to the SMC algorithm except that it assigns an ancestor lineage keep out of the resample stage. The particle Gibbs sampler treats the particles and weights generated from cSMC as a discrete distribution approximating the true density; a

draw is randomly sampled from these particles according to the their weights. Since the draws are obtained from an approximate distribution and not the real one, a pre-specified ancestor lineage or trajectory path is used to guide draws from the invariant unconditional distribution. However, this method is known to have degenerate issues and a poor mixing rate. A finer algorithm is to allow the pre-defined ancestor lineage to update during the forward sampling process, and drop some lineage with degenerate weights. The method is known as particle Gibbs with ancestor sampler (PGAS), proposed by Lindsten et al. (2014). The method uses a trimming technique (Dyk and Park, 2008) to improving the mixing rate of a Gibbs sampler; also, the degenerate weight issue is ameliorated.

In the remainder of this section, we shall introduce this method. We summarize the notations to be used later for convenience: let $q_{-\boldsymbol{\beta}}(\beta_t|Y_t)$ be a proposal density, $\beta_t^1, \ldots, \beta_t^N$ be N particles drawn from the proposal density, k is a index in $\{1, \ldots, N\}$ and $\boldsymbol{k} = (1, \ldots, N)$; let $\boldsymbol{\beta}^k = (\beta_1^k, \ldots, \beta_T^k)$ stand for the samples generated from the same trajectory path k; let $\overline{\boldsymbol{\beta}}_t^k = (\beta_1^k, \ldots, \beta_{t-1}^k, \beta_{t+1}^k, \ldots, \beta_T^k)$, and $\overline{\boldsymbol{k}} = (1, \ldots, k-1, k+1, \ldots, N)$; let β_t' be the previous draws or the starting value for β_t and β_t^* be the current draws from $\beta_t^{\boldsymbol{k}}$; let $w_t(\beta_t^k)$ be the unnormalized weight for the kth particle of β_t sampled from $q(\beta_t| - \boldsymbol{\beta}, Y_t, \beta_{t-1})$, and $W_t(\beta_t^k)$ be its normalized weight.

We consider two methods to choose a proposal density; the first method is to use Taylor expansion on the mean of the observation equation. For simplicity we write (2.2) as the following:

$$
\begin{aligned}
Y_t &= f_{\boldsymbol{\vartheta}}(\beta_t) + \epsilon_t, \\
\beta_t &= g_\phi(\beta_{t-1}) + \eta_t,
\end{aligned}
$$

with $f_{\boldsymbol{\vartheta}}(\beta_t) = \mu + \psi((-\log(\Phi(\beta_t)))^{-\xi} - 1)/\xi$ and $g_\phi(\beta_{t-1}) = \phi\beta_{t-1}$; then we approximate $f_{\boldsymbol{\vartheta}}(\beta_t)$ with

$$
f_{\boldsymbol{\vartheta}}(\beta_t) = f_{\boldsymbol{\vartheta}}\left(g_\phi(\beta_{t-1}^{\boldsymbol{k}})\right) + f_{\boldsymbol{\vartheta}}'\left(g_\phi(\beta_{t-1}^{\boldsymbol{k}})\right)\left(\beta_t - g_\phi(\beta_{t-1}^{\boldsymbol{k}})\right)/c.
$$

Because in a nonlinear equation, the second term in the Taylor expansion can be relatively large, the constant c is used to control the approximated density. We adjust the value c to keep the weights from degenerating. Then the proposal density then can be transformed into a Gaussian

distribution,

$$q_{-\boldsymbol{\beta}}(\beta_t|\boldsymbol{Y}) = N(\nu_{\beta_t}, \sigma^2_{\beta_t})$$

with

$$\sigma^{-2}_{\beta_t} = \frac{1}{(1-\theta^2)} + f'_{\boldsymbol{\vartheta}}(g_\phi(\beta^{\boldsymbol{k}}_{t-1}))^2/\sigma^2$$

$$\nu_{\beta_t} = \frac{\sigma^2_{\beta_t}}{(1-\theta^2)}g_\phi(\beta^{\boldsymbol{k}}_{t-1}) + \frac{f'_{\boldsymbol{\vartheta}}(g_\phi(\beta^{\boldsymbol{k}}_{t-1}))^2}{\sigma^2}\left(Y_t - f_{\boldsymbol{\vartheta}}(g_\phi(\beta^{\boldsymbol{k}}_{t-1})) \times g_\phi(\beta^{\boldsymbol{k}}_{t-1})\right)$$

The second method is to ignore the ϵ_t in (2.2), then we write β_t as a function of y_t as follows,

$$\beta_t = \Phi^{-1}\left(exp\left(-\left(1 + \xi\frac{Y_t - \mu}{\psi}\right)^{-\frac{1}{\xi}}_+\right)\right)$$

where Φ^{-1} denotes the inverse standard normal distribution function. Then we choose a proposal density to be the t-distribution with mean β_t and a small value of degrees of freedom, namely 5. This method does not apply to general state space models, but can perform very well in our model; this is because the ϵ_t in our model is small.

After specifying the proposal density, the PGAS algorithm is as follows,

- At current iteration i, given $\boldsymbol{\beta}'$

- For $t = 1$

    - Draw $\beta_1^{1:N-1} \sim q_{-\boldsymbol{\beta}}(\beta_1|Y_1)$

    - Let $\beta_1^N = \beta_1'$

    - Calculate weight for $l = 1, \ldots, N$ as

$$w_1^l := \frac{f(Y_1|\beta_1^l, \boldsymbol{\vartheta}, \sigma^2)\pi(\beta_1^l)}{q_{-\boldsymbol{\beta}}(\beta_1^l|Y_1)}$$

$$W_1^l = \frac{w_1^l}{\sum_{l=1}^l w_1^l}$$

- For $t = 2, \ldots, T$

    - Resample β_{t-1}^k according to the weight W^k for $k = 1, \ldots, N-1$, denote as $\tilde{\beta}_{t-1}^k$.

10

– Sample $\tilde{\beta}_{t-1}^N$ from $\beta_{t-1}^{\boldsymbol{k}}$ with the associated weights:

$$\frac{w_t^l f(\beta_t'|\beta_{t-1}^l, \phi)}{\sum_{l=1}^N w_t^l f(\beta_t'|\beta_{t-1}^l, \phi)}$$

– Draw $\beta_t^{1,\ldots,N-1} \sim q_{-\boldsymbol{\beta}}(\beta_t|y_t)$

– Let $\beta_t^{iN} = \beta_t'$

– Let $\beta_{1:t}^l := (\tilde{\beta}_{1:t-1}^l, \beta_t^l)$, for $l = 1, \ldots, N$

– Calculate weight for $l = 1, \ldots, N$ as

$$w_t^l = \frac{f(Y_t|\beta_t^l, \boldsymbol{\vartheta}, \sigma^2) p(\beta_t^{il}|\tilde{\beta}_{t-1}^{il}, \phi)}{q_{-\boldsymbol{\beta}}(\beta_t^{il}|Y_t)}$$

$$W_t^l = \frac{w_t^l}{\sum_{l=1}^l w_t^l}$$

- Draw k from $1, \ldots, N$ with the corresponding probability $W_T^{1,\ldots,N}$

- Let $\boldsymbol{\beta} = \boldsymbol{\beta}^k$

- Set $\boldsymbol{\beta}' = \boldsymbol{\beta}$, and go to the next iteration.

Then from the algorithm, we obtain draws for $\boldsymbol{\beta}$.

3.5   Markov Chain Monte Carlo

In summary, the MCMC algorithm is conducted as follows:

1. initialize all the parameters values $\boldsymbol{\vartheta}$, $\boldsymbol{\beta}$, ϕ, σ^2;

2. sample $\boldsymbol{\vartheta} = (\mu, \psi, \xi)$ from (3.1), and using M-H algorithm;

3. sample σ^2 from (3.2);

4. sample ϕ from (3.3), and using M-H algorithm;

5. sample $\boldsymbol{\beta}$ using PGAS;

6. repeat steps 2 — 5 until sufficient draws have been obtained.

4 Seasonal dGEV model

Seasonality can be easily incorporated into our model by adding sinusoids to any of the location, shape or scale parameters. This method is convenient since it has flexibility in the choice of the number of sinusoids and it does not greatly increase the difficulty of making inferences about the model.

We start by adding two sinusoids to the location parameter; the model is shown as follows:

$$
\begin{aligned}
Y_t &= \mu + a_1 \cos(\omega t) + a_2 \sin(\omega t) \\
&\quad + \psi \frac{(-\log(\Phi(\beta_t)))^{-\xi} - 1}{\xi} + \epsilon_t, \ \epsilon_t \sim N(0, \sigma^2), \\
\beta_{t+1} &= \phi \beta_t + \eta_t, \ \eta_t \sim N(0, 1 - \phi^2),
\end{aligned}
\tag{4.1}
$$

where $\omega = 2\pi f$ is the angular frequency, f is the number of cycles that occur for each period of time. For a given dataset, f is typically known; for example, it has value $1/365.25$ for annual variability in a daily dataset, or $1/4$ for a annual variability in a seasonal dataset. In equation (4.1), $t = 1, \ldots, T$, a_1 and a_2 are the coefficients for the two components of the sinusoid, and we let $\boldsymbol{a} = (a_1, a_2)$.

To estimate the parameters in (4.1), we use similar priors to those for the parameters described in Section 3. For the added parameters in the seasonal component in this model, we treat ω as a known parameter. We observe that $\boldsymbol{a}$ has a multivariate normal likelihood in the equation, we choose the prior for each element a_i to be $N(0, \sigma_{a_i}^2)$. Then the posterior for $\boldsymbol{a}$ is as follows,

$$
\pi_{-\boldsymbol{a}}(\boldsymbol{a}|\boldsymbol{Y}) \sim \text{MVN}(\boldsymbol{\nu_a}, \boldsymbol{\Sigma_a})
\tag{4.2}
$$

with

$$
\boldsymbol{\Sigma_a}^{-1} = \sigma^{-2}(\sum_{t=1}^T \boldsymbol{p}_t \boldsymbol{p}_t' + \sigma^2 \boldsymbol{\Omega}^{-1}), \quad \boldsymbol{\nu_a} = \boldsymbol{\Sigma_a}(\sum_{t=1}^T \boldsymbol{p}_t \tilde{Y}_t)/\sigma^2
$$

where $\boldsymbol{p}_t = (\cos(\omega t), \sin(\omega t))^T$, $\boldsymbol{\Omega} = \text{diag}(\sigma_{a_1}^2, \sigma_{a_2}^2)$, $\tilde{Y}_t = Y_t - \mu - \psi \times ((-\log(\Phi(\beta_t)))^{-\xi} - 1)/\xi$. To conduct an MCMC algorithm for this model, we could adapt the algorithm described in Section 3.5, adding an extra step to sample $\boldsymbol{a}$.

12

Sometimes, a dataset may show seasonality in the scale parameter, such as in a weather dataset, the variation in the winter may be larger than in the summer. Our model has the flexibility to deal with a dataset like this by adding two similar sinusoids to ψ, i.e. $\psi + a_3 \cos(\omega t) + a_4 \sin(\omega t)$. It is possible to add sinusoids to the ξ parameter or adding more sinusoidal components to each parameter; however, more parameters in the model will reduce the mixing rate between chains in the MCMC algorithm; as we will shown in the simulation study, the dGEV model already exhibit a large autocorrelation between samples in the chain. For simplicity, we add seasonality only to the location parameter. In the later context, we will refer this model to be the seasonal dGEV model; however, it should be kept in mind that seasonality could be added to any of the parameters.

5 Illustrative simulation study

In this section, we illustrate the dGEV model and seasonal dGEV model (4.1) using simulated data. To generate datasets, we start by generating time-varying parameters $\beta_{1:T}$, and then use $\beta_{1:T}$ to generate observations $Y_{1:T}$.

To be more specific, for the dGEV model, we generate 1000 observations. The choice of the sample size is arbitrary; however, more observations are rquired for a model with more parameters, for example in the case where we add seasonality to both the location and scale parameters. In the simulations, we choose $\phi = 0.8$, $\mu = 0.5$, $\psi = 0.3$ $\xi = 0.05$, and $\sigma = 0.1$. We first simulate $\beta_1 \sim N(0,1)$, then $\beta_2, \ldots, \beta_T$ can be generated according to the AR(1) process in (2.1). Based on the generated values of $\beta_{1:T}$, we then generate dataset $Y_{1:T}$ from (2.2). For the seasonal dGEV model 4.1, we choose $a_1 = 1$, $a_2 = 2$, and suppose we have an annual dataset, $f = 1/365.25$ and $\omega = 2\pi/365.25$.

After generating observations, we need to chose priors to conduct the Bayesian analysis. The priors for those parameters are as follows: $\mu \sim N(0, 2^2)$, $\psi \sim \text{Gamma}(2,2)$, $\xi \sim N(0, 2^2)$, $\phi \sim \text{uniform}(-1,1)$, and $\sigma^2 \sim \text{IG}(1, 0.01)$. We choose the total iteration for MCMC to be 20,000, when running the algorithm, with the first 5,000 as burnin. In the PGAS step, we need to choose number of particles; here we choose the number to be 1000. Lindsten et al. (2014) shows that when this rate is chosen, the PGAS algorithm has update frequency very close to 0.999, the ideal rate.
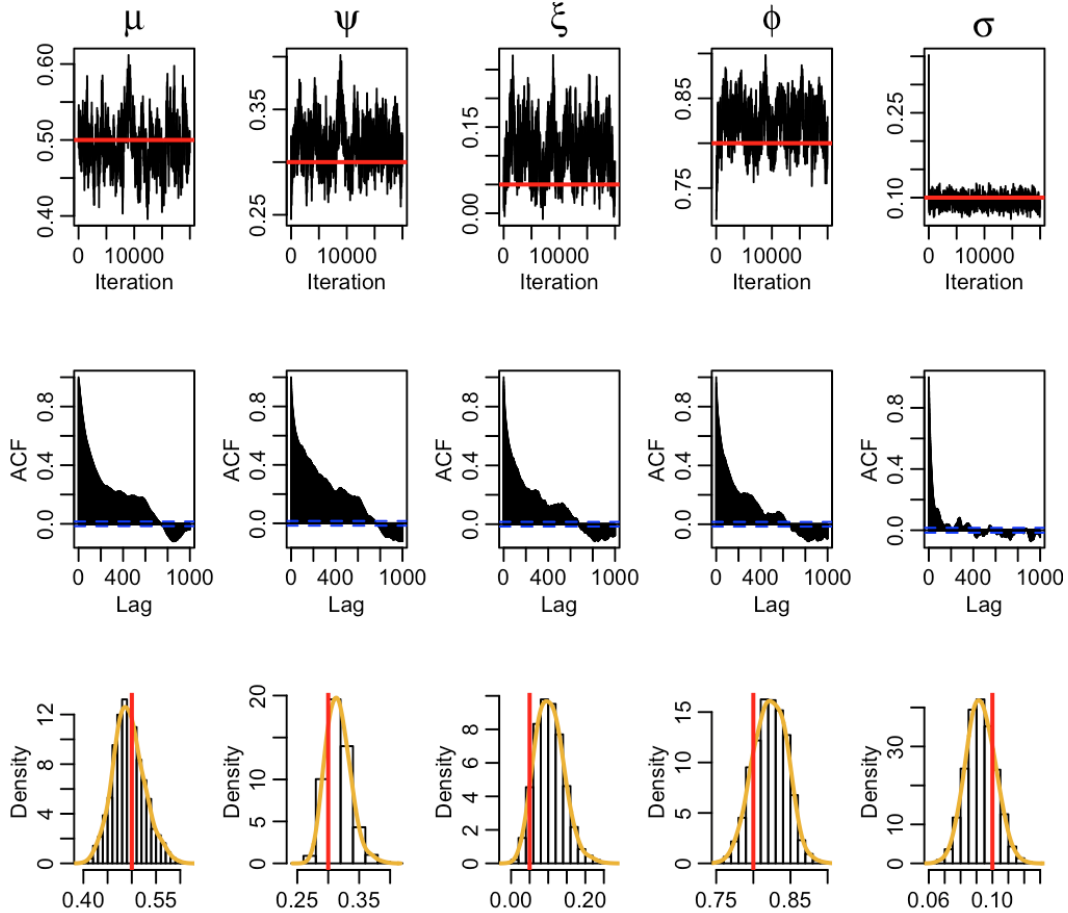
Figure 5.1: Plot of MCMC draws (1st row), autocorrelation function (ACF) (2nd row) and histogram with density (3rd row) for μ, ψ, ξ, ϕ, σ. The red line indicates the true values.

We then fit the model to the simulated datasets. The first row in Figure 5.1 plots the MCMC draws for parameters except for βs for the dGEV model. The draws converge quickly for each parameter; the red lines that indicate the true values are all contained in the draws. Table 5.1 gives summary statistics for the posterior medians and credible intervals. The results show that the true values lie within the 95% credible intervals, and the posterior medians are close to their true values, except for the parameter ξ. The issue with ξ, the shape parameter in the GEV distribution, is that the proposed distribution is a less accurate approximation to the true posterior distribution than in the case of the location and scale parameters; thus its the posterior median has larger bias compared with the posterior medians of μ and ψ.

Table 5.1 also provides the inefficiency factor for each parameter; this statistic gives a diagnostic about how well the chains in MCMC mixed. It is calculated as $1 + 2\sum_{s=1}^{M}(1 - s/M)\rho_s$, as given

14

Table 5.1: Posterior medians and 95% credible intervals for parameters μ, ψ, ξ, ϕ, σ.

Parameter	True value	Posterior median	95% Credible interval	Inefficiency factor
μ	0.5	0.492	[0.4332, 0.5642]	222.26
ψ	0.3	0.315	[0.2818, 0.3599]	233.84
ξ	0.05	0.101	[0.035, 0.1843]	186.26
ϕ	0.8	0.823	[0.7781, 0.8636]	173.69
σ	0.1	0.092	[0.0753, 0.1109]	61.61
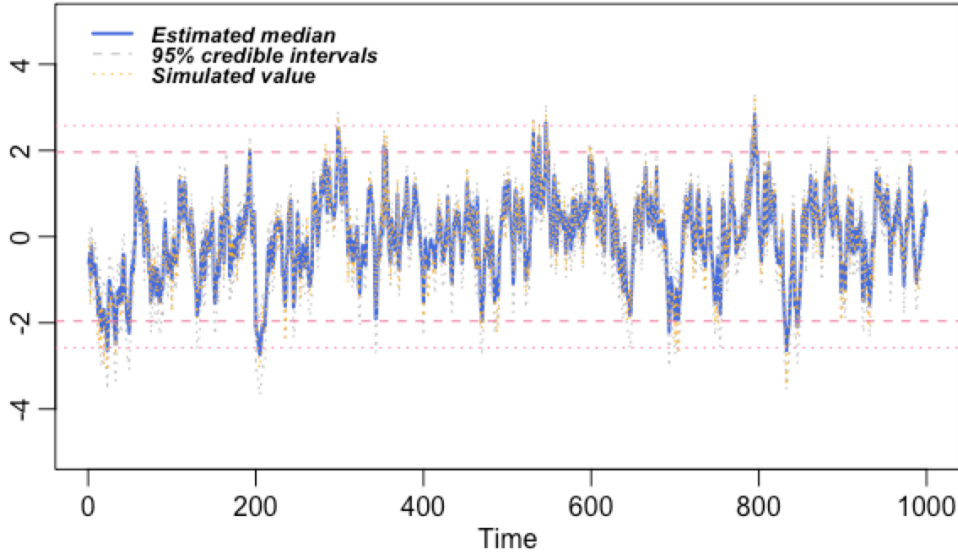
Figure 5.2: Plot of posterior median (blue line) and 95% credible intervals (grey dash lines) for $\beta_1, \ldots, \beta_{1000}$; the yellow dashed lines indicates our simulated value for βs; the four dash red lines from up to down represent the 0.995, 0.975, 0.025, 0.005 quantiles of the standard normal distribution.

by Chib (2001), where ρ_s is the estimated autocorrelation at lag s, and M is the batch size, which we take as 500. An inefficiency factor of m means that the effective number of draws is the total number of iterations, after deleting burnin, divided by m. The results in the table show that those inefficiency factors are large, which corresponds to the slow decay in the ACF plots in Figure 5.1.

Figure 5.2 plots the posterior median and 95% credible intervals for $\beta_1, \ldots, \beta_{1000}$. Recall that the time-varying parameters are in a standard normal copula; thus each β_t has a marginal standard normal distribution. Examining the posterior medians of βs shows that the majority of them fall in the 95% standard normal interval. The credible intervals are very small around each posterior median, as a result of the small value of measurement error ϵ_t.

Figure 5.3 shows the simulation results of selected parameter draws based on the seasonal
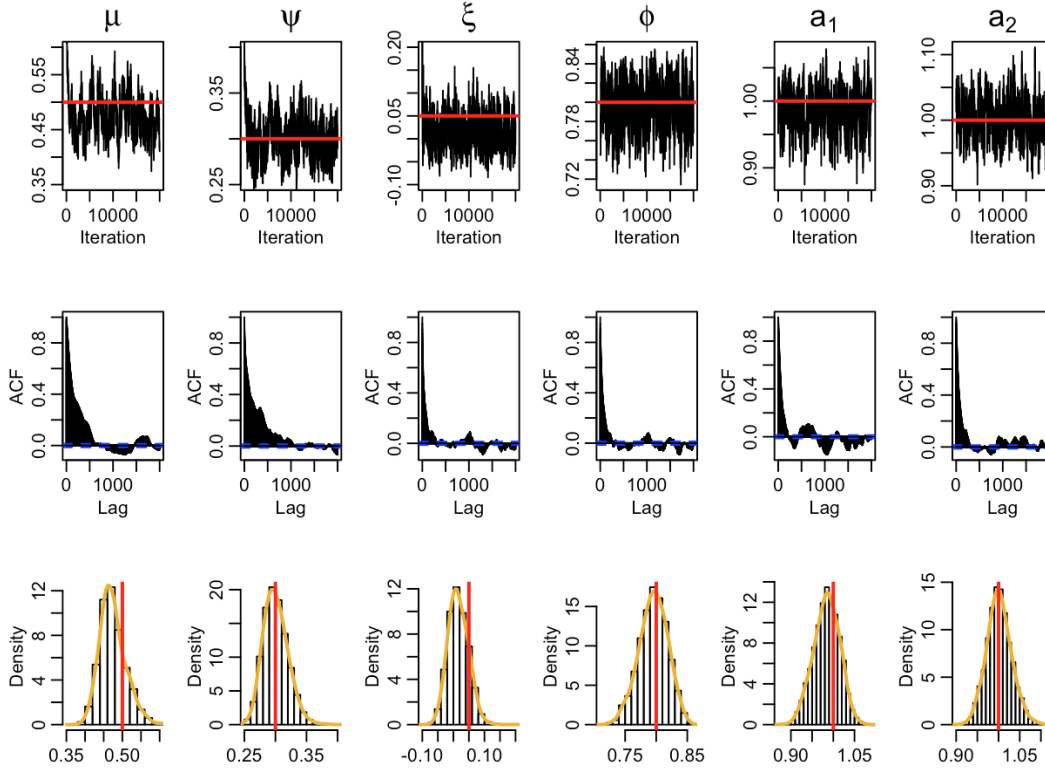
Figure 5.3: Plot of MCMC draws (1st row), autocorrelation function (ACF) (2nd row) and histogram with density (3rd row) for μ, ψ, ξ, ϕ, a_1, a_2. The red line indicates the true values.

dGEV model. The estimated posterior median and 95% credible intervals of those parameters are summarized in Table 5.2. The 95% credible intervals all covered the true value, and posterior medians are close to their true value. Similar to the non-seasonal model, ψ has larger bias compared with μ and ψ. We also found the inefficiency factor for parameters in the seasonal dGEV model to be on average higher than the non-seasonal model; this is because having more parameters in the model increases the correlations between chains. Figure 5.4 gives a plot of posterior medians and their credible intervals for $\beta_1, \ldots, \beta_{100}$. The figures show that the majority of draws fall in the 95% region of the standard normal distribution. Also we plot the simulated true data of $\beta_1, \ldots, \beta_{1000}$ in Figure 5.2; all the true values are covered by their estimated 95% credible intervals.

16

Table 5.2: Posterior median and 95% credit intervals for parameters μ, ψ, ξ, ϕ, a_1, a_2, σ.

Parameter	True value	Posterior median	95% Credible interval	Inefficiency factor
μ	0.5	0.472	[0.4172, 0.5485]	219.05
ψ	0.3	0.300	[0.2681, 0.3396]	214.55
ξ	0.05	0.014	[−0.0432, 0.08136]	92.22
ϕ	0.8	0.797	[0.7486, 0.8380]	103.36
a_1	0.1	0.984	[0.9212, 1.0409]	115.30
a_2	0.1	1.000	[0.9453, 1.0641]	129.67
σ	0.1	0.092	[0.0775, 0.1064]	101.07
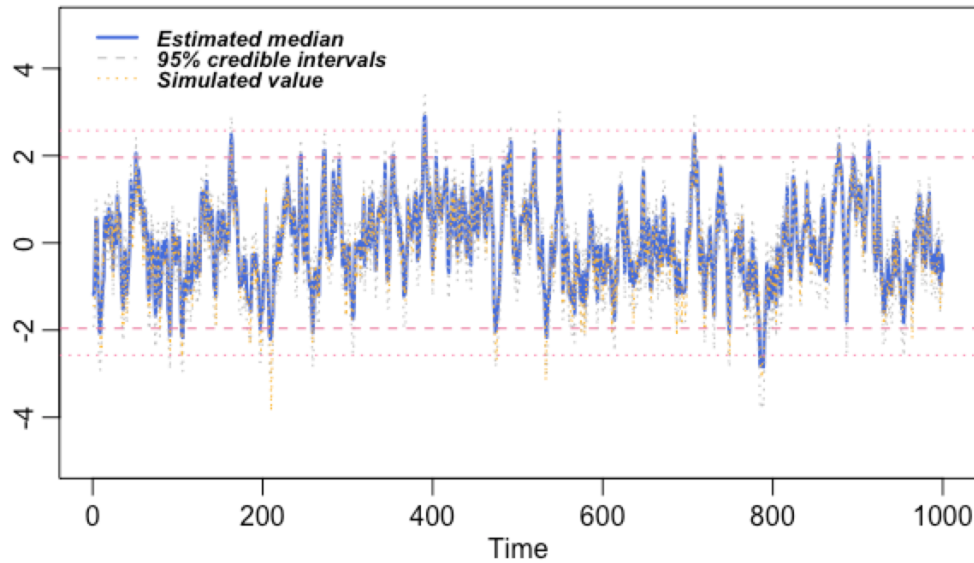
Figure 5.4: Plot of posterior median (blue line) and 95% credible intervals (grey dash lines) for $\beta_1, \ldots, \beta_{1000}$; the yellow dashed lines indicates our simulated value for βs; the four dash red lines from up to down represent the 0.995, 0.975, 0.025, .005 quantiles of the standard normal distribution.

6 Real data study

We will conduct a study of two real datasets in this section. The first dataset is an annal maximum water flow dataset and the second is a minimum log-return dataset for the S&P 500 stock index. We fit the dGEV model to both datasets, and we fit the seasonal dGEV model to the S&P 500.

6.1 Water flow data

A water flow dataset is collected from French Broad River at Asheville in North Carolina. The datasets contains annual maximum water flow level from 1941 to 2009. A plot of this dataset is shown in Figure 6.1, the plot shows there are two spikes in the year 1964 and 2004 which may consider to be unusual years. Our goal is to investigate how extreme those two values could be by fitting into the dGEV model.

We run the chain for 20,000 draws and treat the first 5,000 as burnin, the number of particles is chosen to be 1000. Before running the analysis, we standardize the dataset to avoid computation problem. The plot of draws and summary statistics is presented in Figure 6.2 and Table 6.1. The ACF plots and inefficient factors for each parameters shows the chain mixed well.

From Table 6.1, the time varying parameter ϕ has posterior median 0.021, the 95% credible intervals cover with 0, the result suggests the dependency between extreme values are low or possibly does not exist.

In Figure 6.3, we plot the posterior median for β_ts. Since each β_ts has marginal distribution from standard normal, it is convenient to compare these values with standard normal quantiles. If the values is larger than 2.326 in absolute value, then it is beyond 99% quantiles of normal distribution, which may seems unusual. From the plot, both of the two events in 1964 and 2004 we are interested in lies on the boundary of 95% quantile, and their credible intervals are below

Table 6.1: Posterior medians, 95% credible intervals and inefficient factors for parameters μ, ψ, ξ, ϕ, σ.
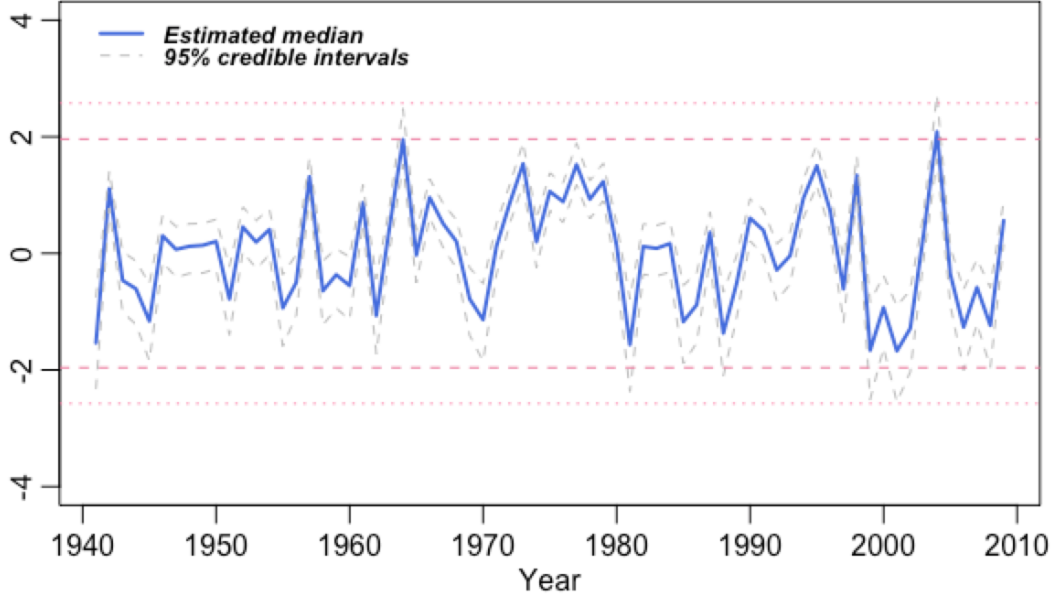
Parameter	Posterior median	95% Credible interval	Inefficiency factor
μ	10144	[8566.1, 118645.0]	170.58
ψ	4351	[3148.0, 6303.0]	223.22
ξ	0.22	[−0.031, 0.664]	223.22
ϕ	0.21	[−0.075, 0.523]	74.16
σ	10.27	[6.468, 19.664]	34.59
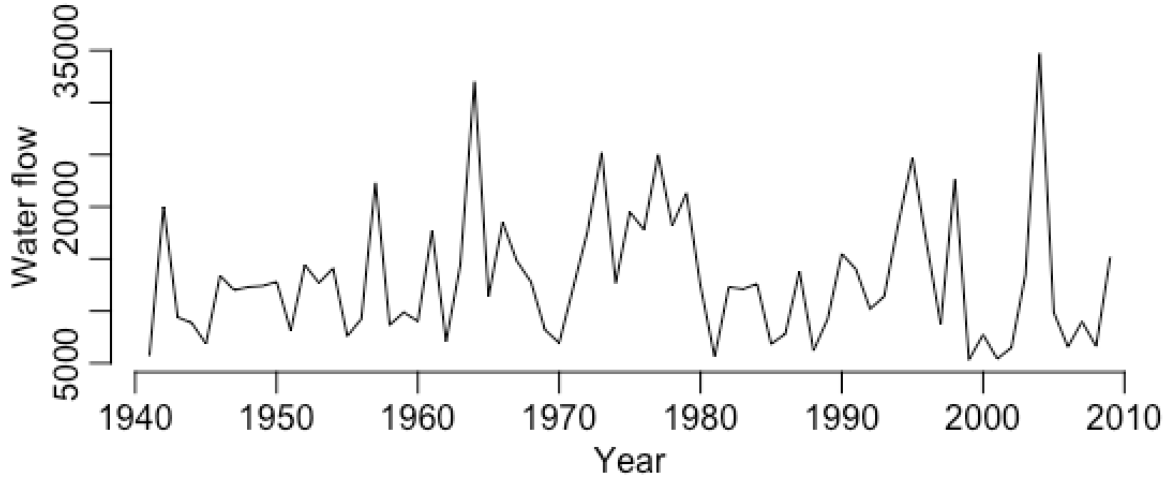
Figure 6.1: Annual maximum water flow of French Broad River at Asheville, North Carolina.
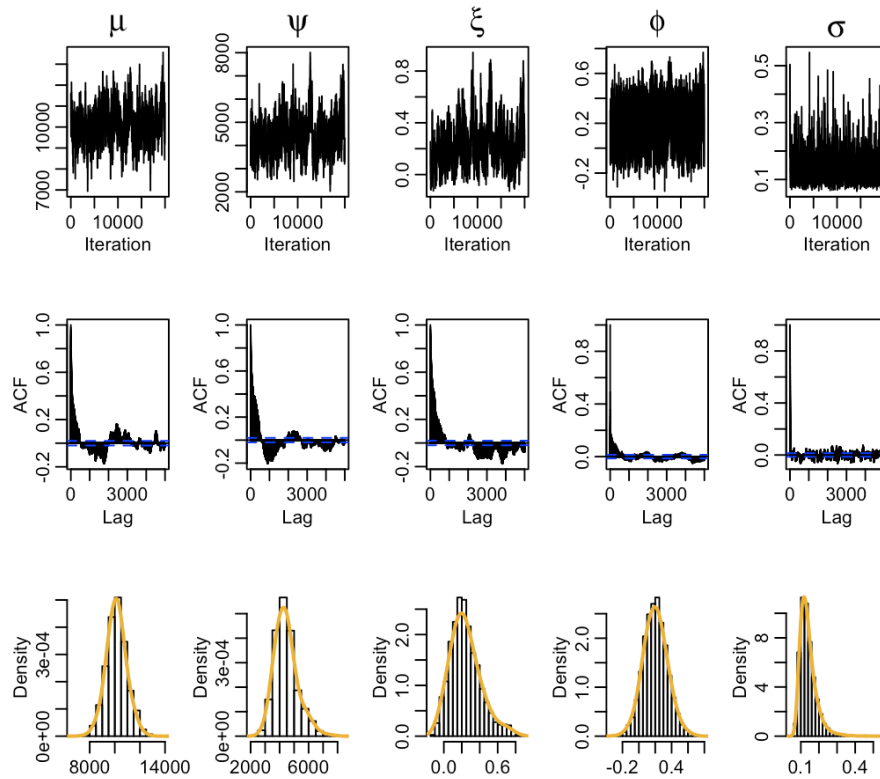
Figure 6.2: Plot of MCMC draws (1st row), autocorrelation functions (ACF) (2nd row) and histograms along with densities (yellow lines) (3rd row) for parameters μ, ψ, ξ, ϕ, σ^2 in dGEV model of the water flow dataset.

Figure 6.3: Plot of posterior medians (blue line) and their 95% credible intervals (grey dash lines) for β_ts by fitting dGEV into water flow dataset. The four dash red lines from up to down represent the 0.995, 0.975, 0.025, 0.005 quantiles of the standard normal distribution.

99% quantile, which may shows the two events are not extreme as it looks like from the data plot.

6.2 S&P 500 datasets

Another dataset is from S&P 500 minimum weekly log-return, the data is collected from September, 25, 2006 to September, 12, 2016. A plot of this data is shown in Figure 6.4. The data is plotted in a -1 scale, so the largest value in the plots stands for the minimum return. Our interests is focus on finding the most unusual happened events in the dataset, especially at the period during 2008 to 2010. Sometimes a time series shows seasonality, although the seasonality is not so obviously to appear in this model, we are interested to fit model to find out if seasonal effects exists. We fit the dataset in both of the dGEV model and the seasonal dGEV model, the plot of draws are shown in Figure 6.5 and Figure 6.6. The posterior medians with their 95% credible intervals for parameters in the model are summarized in Table 6.2. The inefficient factors for those parameters are also provided. In the MCMC algorithm, we run 20,000 iterations and treat the 5000 draws as burnin; we choose the number of particles to be 1000 for both of the two models. For the seasonal dGEV model, we choose $f = 7/365.25$.

From the result shown in Table 6.2, the estimation for location, scale and shape parameters

20
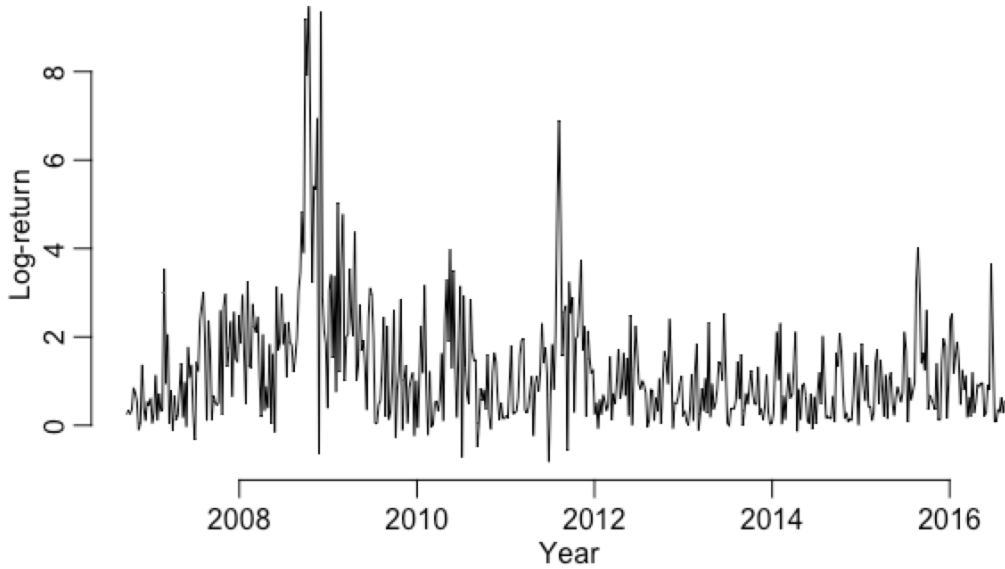
Figure 6.4: Weekly minimum S&P 500 log-return dataset, adjust the dataset to be -1.

for both dGEV and seasonal dGEV model are close, the inefficient factors for seasonal dGEV model are larger than the dGEV model. In the output of the estimation of seasonality parameters a_1, a_2, there value are very close to 0, and their 95% credible intervals contains 0. This suggests seasonality may not exists in this model.

Figure 6.7 gives plot of estimated β_ts posterior medians and their 95% credible intervals for fitting both models. The two models gives a very similar estimates for those β_ts. Both plots indicates the period during 2008 crisis are much more unusual than other period. The highest point has its posterior median close to 99% quantile of standard normal, and its credible intervals bounds contains the area which exceed the 99% quantile.

21
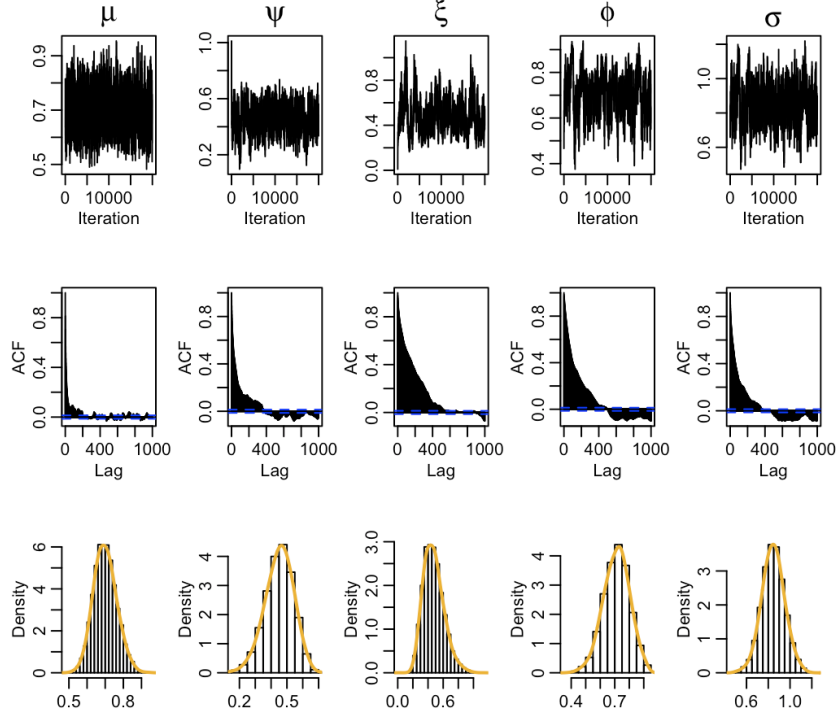
Figure 6.5: Plot of MCMC draws (1st row), autocorrelation functions (ACF) (2nd row) and histograms along with densities (yellow line) (3rd row) for parameters μ, ψ, ξ, ϕ, σ^2 in the dGEV model by fitting the S&P 500 dataset.
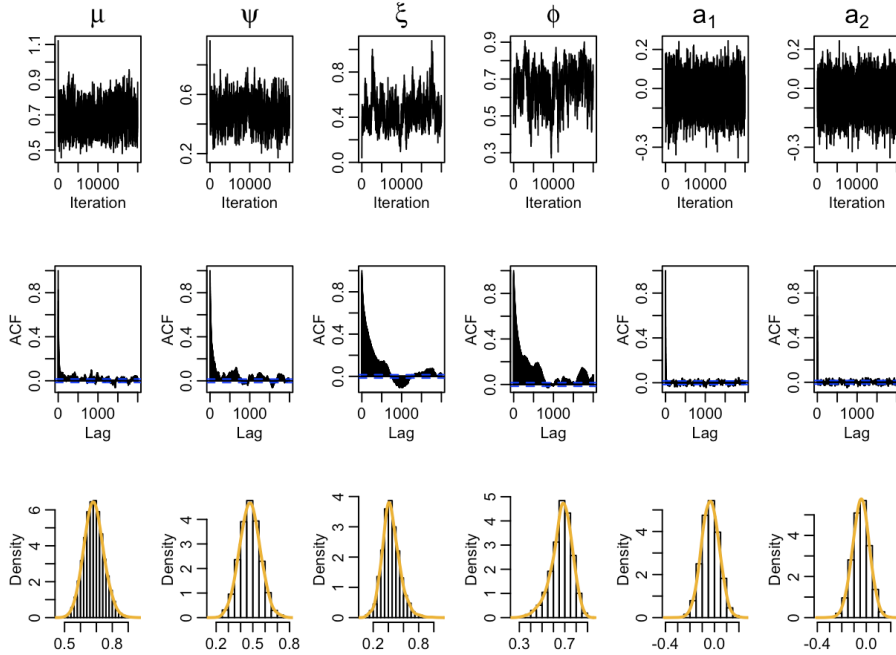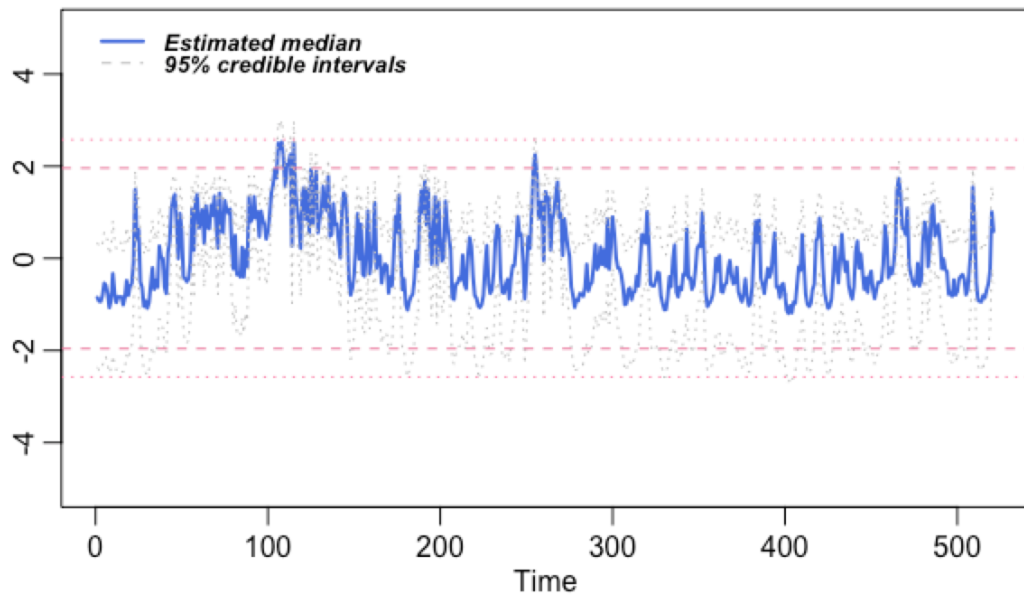

Figure 6.6: Plot of MCMC draws (1st row), autocorrelation function (ACF) (2nd row) and histograms along with densities (yellow line) (3rd row) of parameters μ, ψ, ξ, ϕ, a_1, a_2 in a seasonal dGEV model by fitting the S&P 500 dataset.
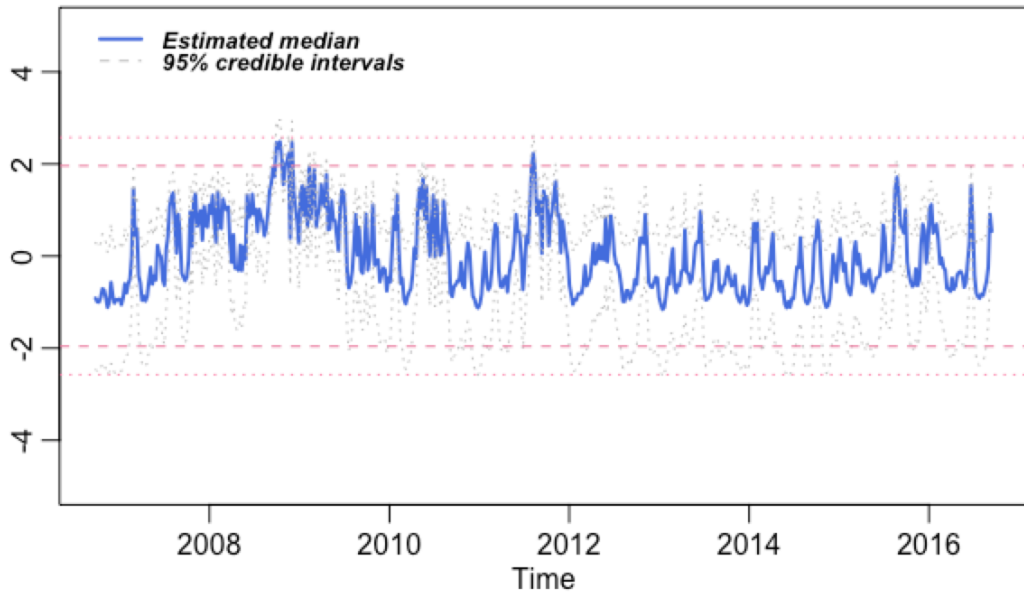
(a)

(b)

Figure 6.7: (a) Plot of posterior medians (blue line) and their 95% credible intervals (grey dash lines) for β_ts by fitting the dGEV model into S&P 500 dataset. (b) Plot of posterior medians (blue line) and their 95% credible intervals (grey dash lines) for β_ts by fitting the seasonal dGEV model into S&P 500 dataset. The four dash red lines from up to down represent the 0.995, 0.975, 0.025, 0.005 quantiles of the standard normal distribution. dataset.

23

Table 6.2: Posterior medians with their 95% credible intervals and inefficient factor for parameters μ, ψ, ξ, ϕ, σ in the dGEV model and parameters μ, ψ, ξ, ϕ, σ, a_1, a_2 in the seasonal dGEV model.

Parameter estimates for dGEV model

Parameter	Posterior median	95% Credible interval	Inefficient factor
μ	0.696	[0.5847, 0.8307]	37.83
ψ	0.348	[0.2171, 0.4645]	80.29
ξ	0.449	[0.2638, 0.7264]	179.25
ϕ	0.713	[0.5347, 0.8555]	145.46
σ	0.967	[0.7425, 1.1817]	96.37

Parameter estimates for seasonal dGEV model

Parameter	Posterior median	95% Credible interval	Inefficient factor
μ	0.683	[0.5691, 0.8101]	39.16
ψ	0.476	[0.3132, 0.6440]	91.94
ξ	0.425	[0.2294, 0.6912]	220.46
ϕ	0.680	[0.4547, 0.8277]	201.65
a_1	−0.034	[−0.1712, 0.1027]	7.75
a_2	−0.042	[−0.1794, 0.0890]	7.76
σ	0.531	[0.3729, 0.6480]	154.70

7 Conclusion and discussion

In this paper, we propose a novel dependent GEV model. The model can be expressed as nonlinear Gaussian state space model. Due to the observation equation is high nonlinear, we use PGAS to sample time-varying parameters. and incorporate it into an MCMC algorithm. The simulation study based on the MCMC algorithm shows the sampled parameter distribution could cover the true value and the posterior median is close to the truth. The shape parameter ξ is turned to be harder to estimate compare to the location and scale parameters. We also show our dGEV model can easily to incorporate seasonal components. Seasonality can be added to both the location, scale and shape parameters.

We did two case studies for the model: one is the annual maximum water flow dataset and another is the weekly minimum return of S&P 500. The estimated dependent parameter in the water flow dataset contains value 0 which suggests the correlation between extreme values are low. The two unusual events in 1964 and 2004 does not turn out to be very unusual after plotting the corresponding estimated value of β. In the S&P 500 dataset, the correlation is very high.

By fitting this dataset into the seasonal dGEV model which suggests there does not exist any seasonality effect. The draws of β_ts shows extreme values during the 2008 economics crisis is very unusual compares to other values.

Our model turns out to require large computation time when the sample size is larger. However, the sample size usually becomes 10,000 when analyzing extremely daily values for temperature. In order to analyze those datasets, a improvement of current algorithm is need. On the other side, for datasets contains seasonality on the scale or shape parameters, the number of parameters will increase and cause the inefficient factors become larger. Thus a method to redesign the MCMC algorithm is needed as well. Both of these issues need to be address in the future study but is beyond the scope of this paper.

References

Andrieu, C., Doucet, A., and Holenstein, R. (2010). Particle Markov chain Monte Carlo methods. *J. R. Statist. Soc. B*, 72:269–342.

Castillo, E., Hadi, A. S., Balakrishnan, N., and Sarabia, J. M. (2004). *Extreme Value and Related Models with Applications in Engineering and Science*. John Wiley & Sons.

Chavez-Demoulin, V. and Davison, A. (2012). Modeling time series extremes. *REVSTAT – Statistical Journal*, 10(1):109–133.

Chib, S. (2001). *Markov chain Monte Carlo methods: computation and inference in Handbook of Econometrics, vol. 5.* Elsevier, North-Holland, Amsterdam.

Chopin, N. and Singh, S. S. (2015). On particle Gibbs sampling. *Bernoulli*, 21(3):1855–1883.

Coles, S. (2001). *Introduction to statistical modeling of extreme values*. Springer-Verlag, London, UK.

Coles, S. G. and Powell, E. A. (1996). Bayesian methods in extreme value modelling: a review and new developments. *International Statistical Review / Revue Internationale de Statistique*, 64(1):119–136.

Coles, S. G. and Tawn, J. A. (1996). A Bayesian analysis of extreme rainfall data. *Journal of the Royal Statistical Society. Series C*, 45:329–347.

Doucet, A. and Johansen, A. M. (2011). A tutorial on particle filtering and smoothing: fifteen years later.

Dyk, D. A. V. and Park, T. (2008). Partially collapsed Gibbs samplers: theory and methods. *Journal of the American Statistics Association*, 103(482):790–796.

Einicke, G. A. and White, L. B. (1999). Robust extended Kalman filtering. *IEEE Transactions on signal processing*, 47.

Huerta, G. and Sansó, B. (2007). Time-varying models for extreme values. *Environmental and Ecological Statistics*, 14:285–299.

Kantas, N., Doucet, A., Singh, S. S., Maciejowski, J., and Chopin, N. (2015). On particle methods for parameter estimation in state-space models. *Statistical Science*, 30(3):328?351.

Lindsten, F., Jordan, M. I., and Schön, T. B. (2014). Particle Gibbs with ancestor sampling. *Journal of Machine Learning Research*, 15:2145–2184.

Lindsten, F. and Schön, T. B. (2013). Backward simulation methods for Monte Carlo statistical inference. *Foundations and Trendső in Machine Learning*, 6(1):1–143.

Liu, J. S. (1994). The collapsed Gibbs sampler in Bayesian computation with applications to a gene regulation problem. *Journal of the American Statistical Association*, 89(427):958–996.

Liu, J. S. (2001). *Monte Carlo Strategies in Scientific Computing*. Springer-Verlag New York, Inc., New York, NY, USA.

Liu, J. S., Wong, W. H., and Kong, A. (1994). Covariance structure of the Gibbs sampler with applications to the comparisons of estimators and augmentation schemes. *Biometrika*, 81(1):27–40.

Nakajima, J., Kunihama, T., and Omori, Y. (2015). Bayesian modeling of dynamic extreme values: extension of generalized extreme value distributions with latent stochastic processes. *Journal of Applied Statistics*, 0(0).

Nakajima, J., Kunihama, T., Omori, Y., and Frühwirth-Schnatter, S. (2011). Generalized extreme value distribution with time-dependence using the AR and MA models in state space form. *Computational Statistics and Data Analysis*, 56(11):3241–3259.

Niemi, J. and West, M. (2010). Adaptive mixture modeling Metropolis methods for Bayesian analysis of nonlinear state-space models. *Journal of Computational and Graphical Statistics*, 19(2):260–280.

Pickands, III, J. (1975). Statistical inference using extreme order statistics. *The Annals of Statistics*, 3(1):119–131.

Shephard, N. and Pitt, M. K. (1997). Likelihood analysis of non-Gaussian measurement time series. *Biometrika*, 84(3):653–667.

Wei, Y. and Huerta, G. (2016). Dynamic generalized extreme value modeling via particle filters. *Communications in Statistics*.

West, M. and Harrison, J. (1997). *Bayesian forecasting and dynamic models (2Nd Ed.)*. Springer-Verlag New York, Inc., New York, NY, USA.

Whiteley, N. (2010). Discussion on the paper "Particle Markov chain Monte Carlo methods". *JRSS-B*, 72(3).